PROCEEDINGS OF THE INTERNATIONAL CONFERENCE NANOMATERIALS: APPLICATIONS AND PROPERTIES
Vol. **3** No 1, 01FNC06(3pp) (2014)

Structure and Properties of Superhard (Zr-Ti-Cr-Nb)N Coatings

B.O. Postolnyi[1,*], O.V. Bondar[1], Yu.A. Kravchenko[1], A.P. Shypylenko[1], O.V. Sobol[2], V.M. Beresnev[3], P. Wegierek[4], K. Smirnova[1], Ya. Kravchenko[1]

[1] *Sumy State University, 2, Rymskogo-Korsakova St., 40007 Sumy, Ukraine*
[2] *National Technical University "Kharkiv Polytechnic Institute", 21, Frunze St., 61002 Kharkiv, Ukraine*
[3] *V.N. Karazin Kharkiv National University, 6, Svobody Sq., 61022 Kharkiv, Ukraine*
[4] *Politechnika Lubelska, 36, Nadbystrzycka St., 20-618 Lublin, Poland*

(Received 22 July 2014; published online 29 August 2014)

This work presents the results of superhard (Zr-Ti-Cr-Nb)N coatings research. Samples were fabricated by vacuum-arc deposition method (Arc-PVD). Structure, composition and properties of these coatings were studied. The study of coatings was performed using SEM, EDS and XRD. Hardness measurements and adhesion tests were provided. The coatings thickness was up to 6.2 μm. Nanocrystallites sizes ranged from 4 to 7.3 nm. Values of hardness and cohesive strength were $H = 43.7$ GPa and $L_C = 62.06$ N respectively. The optimal conditions for coating's deposition were found.

Keywords: Multielement coatings, Nitrides, Hardness, Friction, cohesion, Vacuum-arc deposition.

PACS numbers: 61.46. – w, 62.20.Qp

1. INTRODUCTION

Multilayered and multicomponent materials based on carbides, nitrides, borides and silicides of transition metals are the most promising areas in the study of protective nanocoatings [1-9]. Revealing regularities of structure formation in multielement nitride coatings is necessary for understanding the possibility of controlling the structure and properties of nanomaterials [10-11].

2. EXPERIMENTAL DETAILS

Coatings of (Zr-Ti-Cr-Nb)N system were fabricated by vacuum-arc deposition method (Arc-PVD). Samples were deposited under nitrogen atmosphere using vacuum-arc device "Bulat-6" [12-14]. Evaporated material was a cast in block Zr+Ti+Cr+Nb cathode (composition: Cr – 37.39 at.%, Zr – 27.99 at.%, Nb – 22.30 at.%, Ti – 12.32 at.%) fabricated by electron-beam melting. Table 1 shows physical and technological parameters of coating's fabrication based on (Zr-Ti-Cr-Nb)N system.

Surface morphology of coatings and their elemental composition were studied using scanning electron microscope JEOL-6610 LV and built-in energy dispersive analyzer (X-Max Silicon Drift Detector). Structure and phase composition of coatings were studied by XRD analysis (D8 ADVANCE) in Cu-K_α radiation.

Microhardness of coatings was measured by automated Vickers hardness tester AFFRI DM-8. The imprints were made at the distance of 1.0 mm between each other, 10 measurements were held for each sample. In order to reduce the impact of droplet component and in order to measure the hardness of the coatings more accurately, part of the coatings had been polished after deposition.

Scratch-tester REVETEST (CSM Instruments) was used for adhesion strength study. For this the scratches were made on the surface of the coated samples at continuously increasing load by means of the diamond spherical indenter "Rockwell C" type with a radius of curvature of 200 mm and the following physical parameters were registered: acoustic emission, coefficient of friction and the depth of penetration of the indenter. To obtain the reliable results, two scratches on the surface of the coating were made.

The following critical loads changing the coefficient of friction and acoustic emission curves from the scribing load: L_{C1} - characterizes the time of occurrence of the first chevron crack; L_{C2} - the moment of the appearance of chevron cracks; L_{C3} – the destruction has cohesive and adhesive nature; L_{C4} - local flaking of the areas of the coating; L_{C5} - plastic abrasion of the coating to the substrate.

3. RESULTS AND DISCUSSION

Fig. 1 shows SEM-image of sample #613 surface. Its matrix is based on cells which are typical for surface of vacuum-arc coatings obtained based on nitrides of refractory elements. Furthermore, the coating is composed from rounded inclusions of droplet fraction in diameter up to 6 microns.

Table 1 – Physical and technological parameters of deposition, elemental composition of coatings

#	I_a, A	p_N, Pa	U_b, V	Concentration, at. %							
				Ti	Zr	Cr	Nb	N	C	O	Impurities
613	110	0.3	-100	10.21	6.63	15.22	4.96	18.70	38.29	5.42	0.57
614		0.7	-100	12.30	8.48	16.92	6.17	22.32	27.35	6.46	-
615		0.3	-200	11.27	8.03	18.23	7.48	23.20	31.79	-	-
616		0.7	-200	10.40	7.81	11.00	6.73	22.66	35.63	5.37	0.39
617		0.7	-200	*the pulse stimulation was used*							

* b.postolnyi@gmail.com

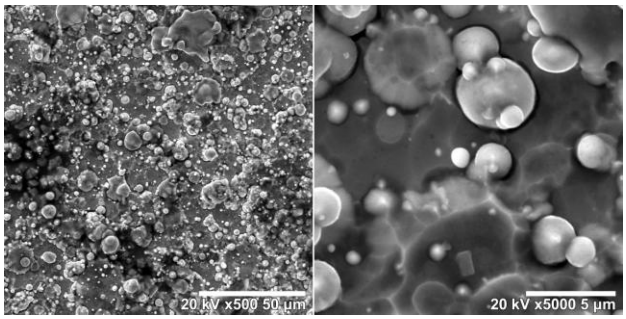

Fig. 1 – The microphotographs of surface (Zr-Ti-Cr-Nb)N coating (sample #613)

The elemental analysis shows that ratio of elements in the composition of material has the same tendency in all obtained coatings: $C_C > C_N > C_{Cr} > C_{Ti} > C_{Zr} > C_{Nb} > C_{impurities}$. Detailed elemental composition of coatings #613-616 is listed in the Table 1. Energy-dispersive X-ray spectrum obtained from the sample #614 (see Fig. 2) confirms the existence of elements presented in Table 1.

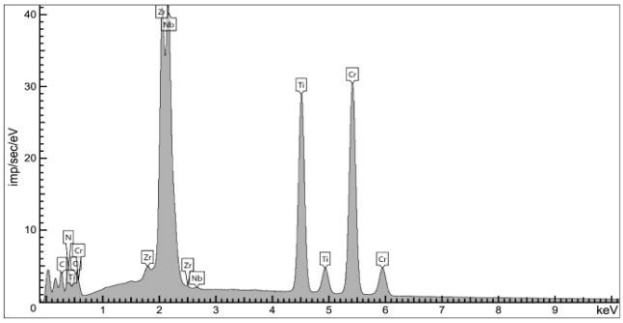

Fig. 2 – The total energy-dispersive X-ray spectrum (sample #614)

Because of the complexity of recognition N, O and C elements using energy-dispersive X-ray spectroscopy one can assume that oxygen is practically absent and nitrogen fraction should be slightly larger due to the reduction of carbon concentration.

Also noteworthy is that Nb and Zr duplicate their position on X-ray maps. Consequently, Nb and Zr form the compounds (perhaps intermetallides) during deposition. We see corresponding drop fraction on the coating surface.

The concentration of nitrogen in the coating increases as the pressure p_N in chamber. The same could be observed with increasing of the negative substrate potential U_b.

The Table 1 also shows the concentration of carbon reduction in samples 614 and 615 which were fabricated at higher nitrogen pressure and substrate voltage respectively. Perhaps it is connected with more compact structure of these samples due to the growth of U_b and p_N.

X-ray diffraction spectra of coatings are shown in Fig. 3. According to X-ray analysis the main phases in the coating may include intermetallic compound of Zr-Cr system. All diffraction peaks corresponding to a low-temperature phase β-$ZrCr_2$ are clearly visible on spectrums. Also lines that correspond to a face-centered cubic lattice of NaCl type are allocated.

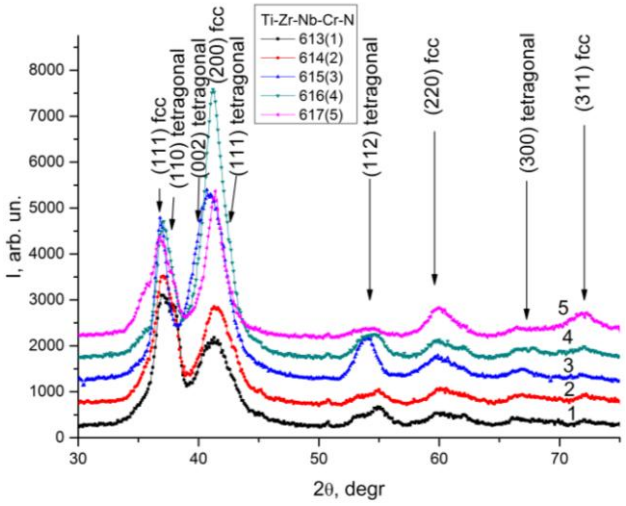

Fig. 3 – X-ray diffraction patterns obtained for samples #613-617

Based on analysis of phase diagrams for the Ti-Zr-Cr-Nb-N system, can be assumed that solid solutions Ti-Zr, Cr-Ti and Cr-Nb may be in coating. Deposition of films in a molecular nitrogen environment, and elemental analysis assumes the formation of the surface nitride compounds. Films deposition in molecular nitrogen atmosphere and elemental surface analysis assume the formation of nitride (Ti, Cr, Nb, Zr)N compounds.

Phase analysis indicates the presence of fcc TiN phase and tetragonal modification of Cr_2N. Increasing of Cr content in the coating leads to diffraction peaks growing (probably due to the influence of tetragonal Cr_2N phase with trigonal lattice and spatial group P31m), with lattice parameters: a = 0.4800 nm and c = 0.4472 nm and extended period from increased nitrogen content (compare spectra 1, 2 and 3-4).

Thus, the three-phase structure of interstitial phases (cubic, tetragonal and hexagonal crystal lattices) forms during deposition.

Period and the crystallite size calculated for fcc lattice is given in Table 2. The crystallite size in more complex tetragonal lattice was about 5 nm.

Table 2 – Size (L) and period of crystallites (for fcc lattice)

Specimen	#613	#614	#615	#616
L, nm	5.2	4.5	5.1	6.9
Period, nm	0.4365	0.4359	0.441	0.4381

Microhardness measurements of samples are presented in Fig. 4. Growth of microhardness observed in coatings with larger crystallite size which were fabricated with increasing nitrogen pressure, increasing bias potential and using impulse stimulation.

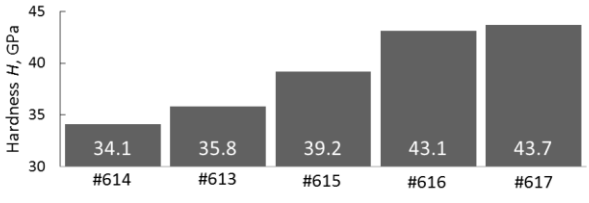

Fig. 4 – Microhardness measurements of coatings

Also, sample #616 became a leader in the adhesive tests (see Fig. 5). Comparative analysis shows that the coatings are erased, but not peeled during scratching (see Fig. 6).

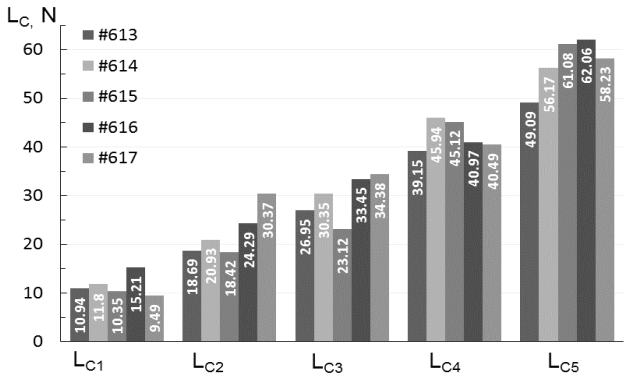

Fig. 5 – Results of adhesion tests

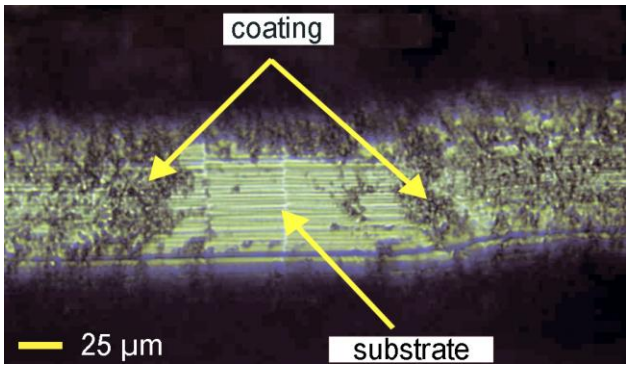

Fig. 6 – The fragment of sample surface after indentation

That is cohesive failure associated with plastic deformation and formation of fatigue cracks in the coating material takes place. The cohesive strength of multicomponent coating (Zr-Ti-Cr-Nb)N was determined from the measurements (L_C=62.06 N).

4. CONCLUSIONS

The hardness of the obtained materials varies depending on the deposition conditions, structure and phase composition. The three-phase structure was formed during deposition of specified systems: with cubic, tetragonal and hexagonal crystal lattices. The maximum hardness was observed in coatings with the biggest crystallites size. They were obtained at high values of the nitrogen pressure in the chamber and substrate potential. The maximum hardness H=43.7 GPa was obtained using impulse stimulation. Indenter load values exceeding the cohesive strength of coatings were L_C=62.06 N.

AKNOWLEDGEMENTS

The work was performed within the framework of comprehensive state program "Development of the basis for formation of multicomponent nanostructured superhard coatings with high physical and mechanical properties" (number 0112U001382) and "Physical principles of plasma technologies for complex processing of multicomponent materials and coatings" (number 0113U000137c).

REFERENCES

1. A.D. Pogrebnjak, A.G. Ponomarev, A.P. Shpak, *Phys. Usp.* **55**, 270 (2012).
2. A.D. Pogrebnjak, V.M. Beresnev, *Nanocoatings Nanosystems Nanotechnologies*, Oak Park, IL: Bentham Science Publishers, (147) 2012.
3. A.D. Pogrebnjak, V.M. Beresnev, A.A. Demianenko, *Phys. Solid State* **54**, 1882-1890 (2012).
4. R. Krause-Rehberg, A.D. Pogrebnyak, V.N. Borisyuk, M.V. Kaverin, A.G. Ponomarev, M.A. Bilokur, K. Oyoshi, Y. Takeda, V.M. Beresnev, O.V. Sobol', *The Physics of Metals and Metallography* **114**, 672-680 (2013)
5. Volodymyr Ivashchenko, Stan Veprek, Alexander Pogrebnjak and Bogdan Postolnyi, *Sci. Technol. Adv. Mater.* **15**, 025007 (2014)
6. A.D. Pogrebnjak, V.M. Beresnev, O.V. Bondar, G. Abadias, P. Chartier, B.A. Postol'nyi, A.A. Andreev, O.V. Sobol' *Techn. Phys. Lett.* **40**, 215 (2014)
7. A.D. Pogrebnyak, M.K. Kylyshkanov, Y.N. Tyurin, A.S. Kaverina, I.V. Yakushchenko, A.A. Borisenko, B.A. Postol'ny, I.A. Kulik *Techn. Phys.* **57**, 840 (2012)
8. A.D. Pogrebnjak, A.P. Shpak, N.A. Azarenkov, V.M. Beresnev, *Phys. Usp.* **52**, 29 (2009).
9. M.K. Kazmanli, M. Urgen, A.F. Cakir, *Surf. Coat. Tech.* **167**, 77 (2003).
10. O.V. Bondar, A.A. Andreyev, B.A. Postolnyi, G. Abadias, V.M. Beresnev, O.V. Sobol, *CriMiCo 2013 - 2013 23rd International Crimean Conference Microwave and Telecommunication Technology, Conference Proceedings*, 865 (2013).
11. A.D. Pogrebnjak, S.N. Bratushka, B.I. Boyko, I.V. Shamanin, Yu.V. Tsvintarnaya *Nucl. Instrum. Methods Phys. Res.* **145**, 373 (1998)
12. A.D. Pogrebnjak, Yu.A. Kravchenko, S.B. Kislitsyn, Sh.M. Ruzimov, F. Noli, P. Misaelides, A. Hatzidimitriou *Surf. Coat. Technol.* **201**, 2621 (2006)
13. A.D. Pogrebnjak, A.D. Mikhaliov, N.A. Pogrebnjak Jr., Yu.V. Tsvintarnaya, V.I. Lavrentiev, M. Iljashenko, A.N. Valyaev, S. Bratushka, A. Zecca, R. Sandrik *Phys. Lett. A* **241**, 357 (1998)
14. A.D. Pogrebnjak, A.V. Pshyk, V.M. Beresnev, B.R. Zhollybekov *J. Friction Wear* **35**, 55 (2014)